Magnetic Reconnection Triggering Magnetohydrodynamic Instabilities during a Sawtooth Crash in a Tokamak Plasma

I. T. Chapman,[1] R. Scannell,[1] W. A. Cooper,[2] J. P. Graves,[2] R. J. Hastie,[1] G. Naylor,[1] and A. Zocco[1]
[1]EURATOM/CCFE Fusion Association, Culham Science Centre, Abingdon, Oxon OX14 3DB, United Kingdom
[2]CRPP, Association EURATOM/Confédération Suisse, EPFL, 1015 Lausanne, Switzerland
(Received 8 October 2010; published 13 December 2010)

Thomson scattering measurements with subcentimeter spatial resolution have been made during a sawtooth crash in a Mega Ampere Spherical Tokamak fusion plasma. The unparalleled resolution of the temperature profile has shed new light on the mechanisms that underlie the sawtooth. As magnetic reconnection occurs, the temperature gradient at the island boundary increases. The increased local temperature gradient is sufficient to make the helical core unstable to ideal magnetohydrodynamic instabilities, thought to be responsible for the rapidity of the collapse.

DOI: 10.1103/PhysRevLett.105.255002 PACS numbers: 52.55.Fa, 52.35.Py

Magnetic reconnection is the phenomenon of the breaking and rejoining of magnetic field lines in a plasma. Examples of this process are solar flares in astrophysical plasmas [1] and the sawtooth instability in tokamak plasmas [2]. While the sawtooth instability was first observed in 1974 [3], the process by which this periodic collapse of the core plasma temperature occurs is still only partially understood. Diagnosis of the sawtooth crash has shown that the temperature profile is initially axisymmetric but is deformed by a helical instability before a rapid temperature collapse reestablishes an axisymmetric profile with a lower value at the magnetic axis [4].

Tokamak plasmas are susceptible to sawtooth oscillations when the safety factor $q = d\psi_\phi/d\psi_\theta$ is less than unity [5], where ψ_ϕ and ψ_θ are the toroidal and poloidal magnetic fluxes, respectively. The helical perturbation which arises during the crash has an $m = n = 1$ structure, where m and n are the poloidal and toroidal periodicity of the wave, respectively. The first explanation of the periodic temperature collapses was proposed by Kadomtsev [2], who showed that reconnection occurs at the separatrix on the characteristic Sweet-Parker time scale [1] $\tau_K = \sqrt{\tau_R \tau_A} = \tau_A \sqrt{S}$, where $\tau_A = a\sqrt{4\pi\rho} B_\theta^{-1}$ is the poloidal Alfvén time, $\tau_R = 4\pi a^2/\eta c^2$ is the resistive diffusion time, ρ is the mass density, η is the plasma resistivity, and $S = \tau_R/\tau_A$ is the Lundquist number. This time scale is up to 2 orders of magnitude too large to explain crash times in large modern-day tokamaks, where $\tau_{\text{crash}} \sim 20$–$100$ μs, whereas $\tau_K = 2$–10 ms.

The three principal observations which any theory must explain are (i) the rapidity of the temperature collapse, (ii) the sudden onset of the collapse, and (iii) the incomplete relaxation of the current profile whereby q remains below unity while the temperature profile relaxes completely. The incremental change in the safety factor which governs the stability of the $m = n = 1$ mode is too small to explain the rapid onset. Many alternative crash models have been proposed, including resistive two-fluid MHD [6], collisionless kinetic effects [7], accelerated complete reconnection due to nonlinear collisionless effects [8], magnetic stochastization leading to enhanced perpendicular transport [9], widespread magnetic turbulence as the island reaches a critical width [10], and triggering of secondary instabilities [11–13]. Each model has had proponents and experimental support. The collisionless reconnection model mediated by the electron pressure gradient [14] provides a satisfactory explanation of the crash rapidity and the sudden onset but fails to explain the partial reconnection. Similarly, the precipitous drop in the pressure gradient that occurs due to rapid electron heat transport removing the drive for the initial helical perturbation may explain (iii) but not the rapid transition from mode growth to the sudden crash. However, the triggering of a secondary instability [11–13] by the strong pressure gradient arising from reconnection can provide a simultaneous explanation of these phenomena. While previous experimental data have given great insight into the phenomenology of the crash [15,16], it had insufficient radial resolution to provide validation or vitiation of the concept of secondary instabilities [5,12,13], and theoretical or numerical comparison has been stifled by this.

The recently upgraded Thomson scattering (TS) system on the Mega Ampere Spherical Tokamak (MAST) [17], with radial resolution <10 mm and the possibility of a temporal resolution of 1 μs, has allowed detailed analysis of the electron density and temperature profiles during a sawtooth crash. The system is designed to measure at high spatial resolution and achieve low systematic and random errors, allowing observation of changes in the gradients over narrow regions associated with magnetic islands. Figure 1 shows the electron temperature (T_e) profiles measured by the TS at eight time slices, 20 μs apart in MAST shot 24479, from the onset of growth of the $m = n = 1$ island until after the sawtooth crash. In this shot, a localized flattening of T_e occurs as an $n = m = 1$ magnetic island develops. Initially flat spots are visible on both sides

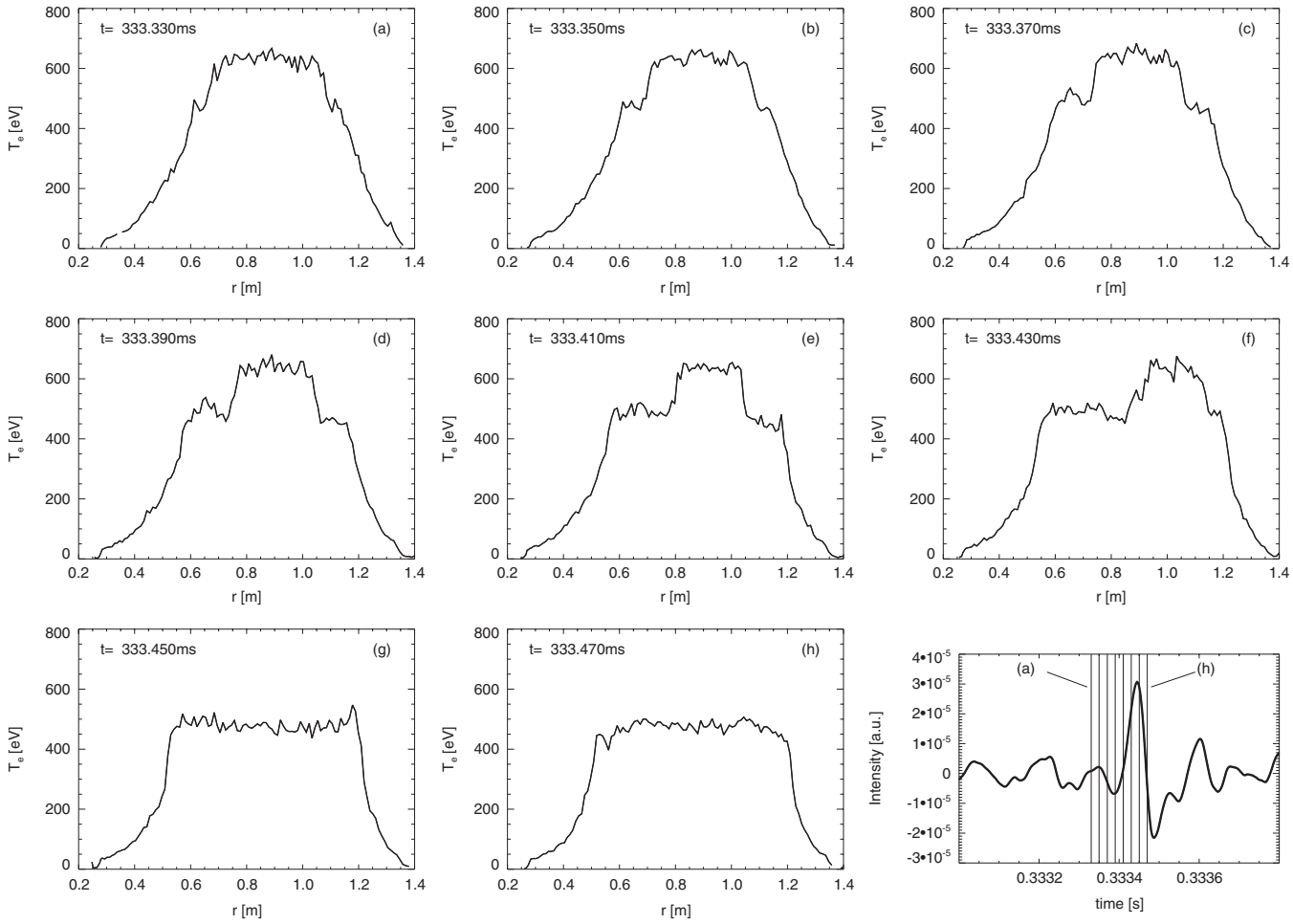

FIG. 1. (a)–(h) show the electron temperature profile every 20 μs across a sawtooth crash measured by the Thomson scattering in MAST discharge 24479. Also shown is the $n =$ odd magnetic signals measured by the Mirnov coils on the outboard midplane.

of the magnetic axis [e.g., Fig. 1(c)] as the diagnostic line of sight passes through two parts of the island crescent. Later, the temperature is flattened primarily on the high-field side [Fig. 1(f)] as the island rotates and the TS views through the island O point. The crash phase occurs between Figs. 1(f) and 1(g), in less than 20 μs. Such local flattening in microsecond time scales was also observed by using electron cyclotron emission measurements with 1–2 cm resolution [18].

In contrast to T_e, the electron density (n_e) profile remains constant during this time, as seen in Fig. 2. The reason for this is likely to be the relative parallel velocities of the ions and electrons. Constant density suggests that full reconnection does not occur, supported by the observation that the safety factor (derived from equilibrium reconstruction with the EFIT code constrained by TS measurements together with magnetic field pitch angle measurements from the motional Stark effect diagnostic) remains below unity after the crash.

Both the growth of the magnetic island width and the eventual crash occur on very rapid time scales: $\sim$100 μs and $\leq$ 20 μs, respectively. The island growth is much quicker than the resistive diffusion time $\tau_r \sim 180$ ms, and the crash occurs much faster than reconnection theory predicts [1]: $\tau_K \sim 340$ μs. This rapid evolution of the island induces a significant increase in the electron temperature gradient at the boundary layer, which is consistent with the physical antecedent necessary for triggering a secondary pressure-driven instability [11–13]. The interaction of the electron cross-field thermal conduction and the reconnection of the magnetic field lines associated

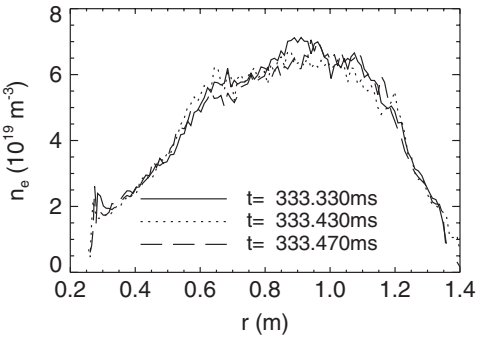

FIG. 2. The electron density profile during MAST shot 24479 remains effectively unaltered while Fig. 1 shows that the electron temperature changes significantly.

with the $m = n = 1$ island can increase both the local pressure gradient at the boundary layer adjacent to the reconnecting layer and the poloidal beta of the core [$\beta_p = (2\mu_0 R^2/r_1^4 B_\phi^2) \int_0^{r_1} drr^2 dp/dr$], which in turn can drive ideal MHD modes on Alfvénic time scales $\tau_A \sim 0.7$ μs. The width of this boundary layer is determined by the ratio of the electron cross-field thermal diffusivity and the speed at which the reconnection progresses [13]. Figure 3 shows the evolution of both the width of the island on low- and high-field sides of the magnetic axis as well as the gradient of the electron temperature at the inner island boundary layer as measured by the TS. As the magnetic island width grows, the electron temperature gradient at the boundary layer increases.

It is possible to estimate the thermal diffusivity at the boundary layer from the reconnection speed and the island width. Reference [13] gives that the temperature gradient in the boundary layer for an initial profile of the form $T = T_0(1 - r/r_1)$ is $dT/dr'|_{r'=r_1-w} \approx (T_0/r_1)/[(r + \Delta)/\Delta]$, where r_1 is the minor radius at $q = 1$, $\Delta = \chi_{e\perp}/V_r$ is the thickness of the boundary layer, $\chi_{\perp e}$ is the electron cross-field thermal diffusivity, V_r is the reconnection speed, and $w = V_r t$ is the incremental width of the island. By considering ∇T_e illustrated in Fig. 3, the electron diffusivity is estimated as $\chi_e = 10$–40 m^2 s^{-1}, which compares favorably with transport simulations constrained to match the experimental neutron rate or gyrokinetic simulations, where $\chi_e \approx 10$ m^2 s^{-1} [19].

The increase in the local pressure gradient in regions of adverse average curvature drives both ballooning modes [11] and interchange MHD instabilities [12]. The drive from the pressure gradient competes with the stabilizing effect of the magnetic shear, $s = r/qdq/dr$, and shaping effects [20]. An average stabilizing magnetic well exists in shaped tokamak plasmas due to the curvature of the system, except well inside $q = 1$ where the average curvature is destabilizing. In these MAST plasmas, not only does the pressure gradient increase as the island grows, but the radial location of the increased temperature gradient moves towards the magnetic axis, i.e., towards a region of lower magnetic shear. This increase in the pressure gradient will not give rise to increased diamagnetic or kinetic stabilization of the interchange mode, since such effects scale with the ion or fast ion pressure gradients, respectively, but only T_e changes on these very fast time scales. The ideal Mercier criterion [21] has been calculated for equilibria with the temperature profiles at each of the time slices in Fig. 1. The q profile is obtained from EFIT reconstruction constrained by motional Stark effect measurements made shortly before the crash and the pressure gradient obtained from TS measurements. During the island evolution the plasma core is assumed to be incompressible, so the enclosed flux in the area of the hot core is the same as before the kink perturbation, allowing the safety factor at the boundary layer to be inferred from the preisland equilibrium. This effectively implies that a current sheet arises at the boundary layer between the core plasma which has $q < 1$ and the separatrix where $q = 1$. The core plasma shape is taken from both the original equilibrium (labeled "low δ") and from the (1, 1) perturbation produced by axisymmetric linear stability analysis ("moderate δ"). A 2D analysis finds ballooning (Fig. 4) and ideal Mercier instability (Fig. 5) by $t = 333.41$ ms. The fact that the Mercier index is well above 0.5 suggests that the mode will grow on Alfvénic time scales. Such explosive growth explains the onset of the crash in $\tau_{\text{crash}} \leq 20$ μs, which is at least an order of magnitude quicker than resistive instability growth or fast magnetic reconnection. Such ideal pressure-driven instabilities propagate the strong pressure gradient towards the axis (since Mercier modes are stable outside $q = 1$) causing a rapid collapse of T_e [12].

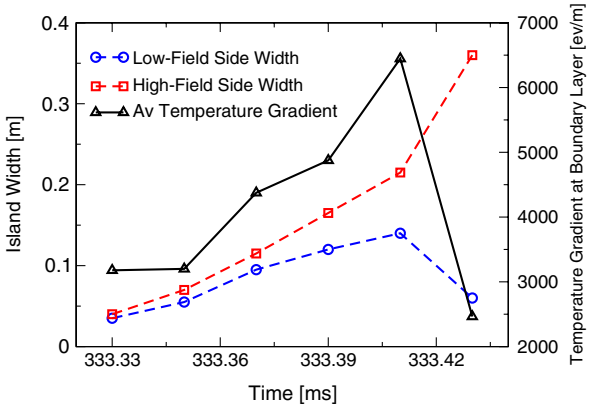

FIG. 3 (color online). The Thomson scattering measurement of the width of the magnetic island on the low- and high-field sides of the magnetic axis together with the T_e gradient at the internal boundary layer as the island evolves for MAST shot 24479.

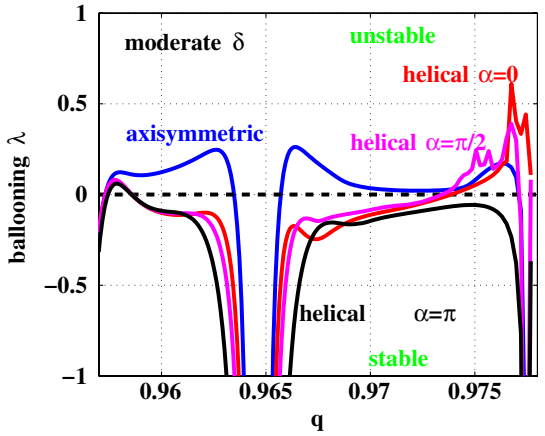

FIG. 4 (color online). The infinite-n ballooning mode growth rate ($\lambda > 0$ is unstable) of MAST discharge 24479 as a function of q for both 2D and 3D treatment of the plasma core at $t = 333.41$ ms. In the 3D case, the stability is shown for different toroidal angles at which the field line crosses the outboard side of a flux surface α. Since the 3D treatment allows for the clustering of flux surfaces on the low-field side due to the perturbation, ballooning modes become more stable in the core but are more unstable at the boundary layer.

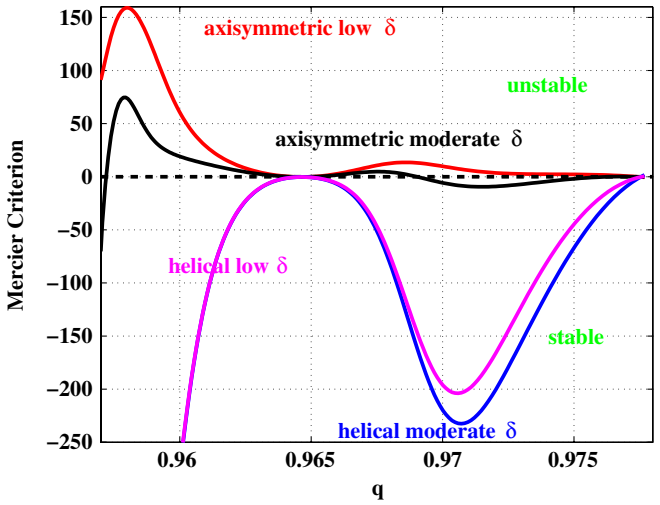

FIG. 5 (color online). The Mercier index defined in Ref. [21] (> 0 is unstable) of MAST discharge 24479 as a function of q for both 2D and 3D treatment of the plasma core at $t = 333.41$ ms. Axisymmetric analysis predicts interchange instability for low shaping and marginal stability at the strongest T_e' for moderate shaping, whereas helical analysis predicts stability everywhere.

A more accurate nonaxisymmetric stability analysis of the kinked equilibrium has been undertaken by using the VMEC 3D equilibrium code [22] and the TERPSICHORE 3D linear stability code [23]. The toroidal variations of the perturbation are taken from an equilibrium which spontaneously develops a bifurcated helical core structure [24]. When the helical $1/1$ perturbation is included, the plasma core becomes stable to ballooning modes except near the boundary layer where instability is exacerbated, since the 3D deformation tends to squeeze the pressure gradient outwards. Conversely, in the shaped MAST plasmas, the helical treatment predicts improved Mercier stability, suggesting that ballooning modes represent a stronger candidate to expedite the crash shown in Fig. 1. While the localized pressure bulges seen experimentally [15] are consistent with ballooning modes, they were sometimes observed to be localized in a region of good curvature, which violates the axisymmetric ballooning theory. The physics is less clear in the helically deformed case where the perturbation will grow where the local shear is weakest and the pressure gradient is strongest. Furthermore, the circular plasmas in Ref. [15] had increased Mercier instability such that interchange modes could have mediated the rapid crash in that case, whereas ballooning modes mediate these shaped MAST plasmas. The increased temperature gradient can also enhance microtearing or kinetic ballooning instability.

Temperature profile measurements with unparalleled spatial resolution have shed new light on the mechanism of the sawtooth crash in tokamak plasmas. An $m = n = 1$ magnetic island grows rapidly, leading to a strong increase in the electron temperature gradient at the island boundary. The island width grows and the region of increasing gradient moves into regions of lower magnetic shear, before the sawtooth crash occurs in less than 20 μs. The nonaxisymmetric plasma in the presence of a growing magnetic island is found to be unstable to interchange or ballooning modes, which are postulated to result in the rapid crash following instability growth on Alfvénic time scales.

The authors acknowledge useful discussions with S. C. Cowley, C. G. Gimblett, S. D. Pinches, and A. Thyagaraja. This work was partly funded by the RCUK Energy Program under Grant No. EP/G003955 and the European Communities under the contract of Association between EURATOM and CCFE. The views and opinions expressed herein do not necessarily reflect those of the European Commission.

[1] E. N. Parker, Astrophys. J. Suppl. Ser. **8**, 177 (1963).
[2] B. Kadomtsev, Sov. J. Plasma Phys. **1**, 389 (1976).
[3] S. von Goeler, W. Stodiek, and N. Sauthoff, Phys. Rev. Lett. **33**, 1201 (1974).
[4] A. W. Edwards *et al.*, Phys. Rev. Lett. **57**, 210 (1986).
[5] M. N. Bussac, R. Pellat, D. Edery, and J. L. Soule, Phys. Rev. Lett. **35**, 1638 (1975).
[6] M. N. Bussac, D. Edery, R. Pellat, and J. L. Soule, Plasma Phys. Controlled Nucl. Fusion Res. **1**, 607 (1976); G. Ara *et al.*, Ann. Phys. (N.Y.) **112**, 443 (1978).
[7] T. Antonsen, B. Lane, and J. Ramos, Phys. Fluids **24**, 1465 (1981).
[8] M. Ottaviani and F. Porcelli, Phys. Rev. Lett. **71**, 3802 (1993).
[9] A. J. Lichtenberg, K. Itoh, S. I. Itoh, and A. Fukayama, Nucl. Fusion **32**, 495 (1992).
[10] F. Porcelli, D. Boucher, and M. N. Rosenbluth, Plasma Phys. Controlled Fusion **38**, 2163 (1996).
[11] M. N. Bussac and R. Pellat, Phys. Rev. Lett. **59**, 2650 (1987).
[12] C. G. Gimblett and R. J. Hastie, Plasma Phys. Controlled Fusion **36**, 1439 (1994).
[13] T. K. Chu, Nucl. Fusion **28**, 1109 (1988).
[14] A. Y. Aydemir, Phys. Plasmas **4**, 3469 (1992); X. Wang and A. Bhattacharjee, Phys. Rev. Lett. **70**, 1627 (1993).
[15] H. K. Park *et al.*, Phys. Rev. Lett. **96**, 195004 (2006).
[16] Y. Nagayama *et al.*, Phys. Plasmas **3**, 1647 (1996).
[17] R. Scannell *et al.*, Rev. Sci. Instrum. **79**, 10E730 (2008).
[18] E. A. Lazarus *et al.*, Phys. Plasmas **14**, 055701 (2007).
[19] R. J. Akers *et al.*, in *Proceedings of the 22nd IAEA Fusion Energy Conference, Geneva, 2008* (IAEA, Vienna, 2008), EX/2-2.
[20] H. Lütjens, A. Bondeson, and G. Vlad, Nucl. Fusion **32**, 1625 (1992).
[21] W. A. Cooper, Plasma Phys. Controlled Fusion **34**, 1011 (1992).
[22] S. P. Hirshman, W. I. Van Rij, and P. Merkel, Comput. Phys. Commun. **43**, 143 (1986).
[23] D. V. Anderson *et al.*, Int. J. Supercomput. Appl. High Perform. Comput. **4**, 34 (1990).
[24] W. A. Cooper *et al.*, Plasma Phys. Controlled Fusion (to be published).